Chemosphere 184 (2017) 1020–1027

Contents lists available at ScienceDirect

Chemosphere

journal homepage: www.elsevier.com/locate/chemosphere

Rhodamine B in dissolved and nano-bound forms: Indicators for light-based advanced oxidation processes

Efrat Shabat-Hadas [a], Hadas Mamane [a], Vitaly Gitis [b, *]

[a] School of Mechanical Engineering, Faculty of Engineering and Water Research Center, Tel Aviv University, Tel Aviv 69978, Israel
[b] Unit of Energy Engineering, Faculty of Engineering Sciences, Ben-Gurion University of the Negev, PO Box 653, Beer-Sheva 84105, Israel

HIGHLIGHTS

- Dyed viruses are usable in evaluation of photodegradation in complex environment.
- Non-toxic $BiOCl_xBr_{1-x}$ is a better photocatalyst than P25 TiO_2.
- UV/H_2O_2 and photocatalysis result in linear degradation of free rhodamine B.
- Adsorption of free rhodamine B on catalyst can influence degradation.
- Nano-bound rhodamine B shows high potential as AOP indicator.

GRAPHICAL ABSTRACT

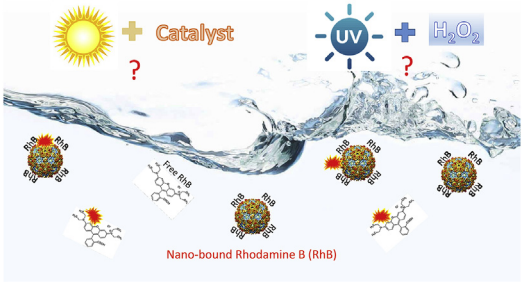

ARTICLE INFO

Article history:
Received 3 April 2017
Received in revised form
12 June 2017
Accepted 17 June 2017
Available online 19 June 2017

Handling Editor: Jun Huang

Keywords:
UV
UV/H_2O_2
Photocatalysis
Rhodamine B
Bismuth
Titanium dioxide

ABSTRACT

Rhodamine B (RhB) is a water-soluble fluorescent dye that is often used to determine flux and flow direction in biotechnological and environmental applications. In the current research, RhB in soluble (termed free) and virus-bound (termed nano-bound) forms was used as an efficiency indicator for three environmental processes. The degradation of free and nano-bound RhB by (i) direct UV photolysis and (ii) UV/H_2O_2 advanced oxidation process (AOP) was studied in a collimated beam apparatus equipped with medium-pressure mercury vapor lamp. The degradation by (iii) solar light-induced photocatalysis was studied in a solar simulator with titanium dioxide and bismuth photocatalysts. Results showed negligible RhB degradation by direct UV and solar light, and its nearly linear degradation by UV/H_2O_2 and photocatalysis/photosensitization in the presence of a solid catalyst. Considerable adsorption of free RhB on bismuth-based catalyst vs. no adsorption of nano-bound RhB on this catalyst or of any form of the dye on titanium dioxide produced two important conclusions. First, the better degradation of free RhB by the bismuth catalyst suggests that close proximity of a catalyst hole and the decomposing molecule significantly influences degradation. Second, the soluble form of the dye might not be the best option for its use as an indicator. Nano-bound RhB showed high potential as an AOP indicator, featuring possible separation from water after the analysis.

© 2017 Elsevier Ltd. All rights reserved.

1. Introduction

Prediction of micropollutant and microorganism degradation by advanced oxidation processes (AOPs) is one of the few remaining unresolved factors in more efficient AOP-based water treatment. AOPs are a family of *in-situ* chemical reactions that are initially

* Corresponding author.
E-mail address: gitis@bgu.ac.il (V. Gitis).

http://dx.doi.org/10.1016/j.chemosphere.2017.06.076
0045-6535/© 2017 Elsevier Ltd. All rights reserved.

united by the formation of highly reactive hydroxyl radicals (•OH). These radicals are often generated by hemolytic cleavage of the O–O bond of hydrogen peroxide (H_2O_2) with UV light. The extended AOP family also includes processes such as ozonation, Fenton reactions, plasma oxidation and solar-driven photocatalysis. AOPs are environmentally friendly methods for the disinfection of pathogenic microorganisms and degradation of organic micropollutants in water (Bahnmuller et al., 2015) and wastewater of both domestic (Zucker et al., 2016) and industrial origins (Oller et al., 2011).

The degree of contaminant degradation by light (UV or solar)-based AOPs in controlled laboratory-scale batch experiments depends on AOP kinetics (i.e. second-order rate constants with •OH), but also on water quality (i.e. •OH radical exposure) and on the concentration of the micropollutant in question. However, in large-scale applications under continuous flow operations, evaluation of AOP efficacy is complicated by the variety of micropollutants present in the water, reactor geometry, flow field, fouling, UV lamp aging or failure, presence of colloidal particles, and calibration of dosing pumps, among others. Consequently, the degree of degradation cannot be predicted, but it can be evaluated. Such an evaluation not only validates system performance but is also required for both plant management and inspecting authorities.

The degree of disinfection/degradation using light-based AOPs can be evaluated by computational fluid dynamics, biodosimetry or chemical actinometry. Computational fluid dynamics predicts disinfection/degradation from trajectories of pollutants fed through an AOP reactor using appropriate hydrodynamic/turbulence models, fluency-rate distribution models, and chemical reaction mechanisms (Bagheri and Mohseni, 2015; Ducoste and Alpert, 2015). Biodosimetry measures the inactivation of a surrogate microorganism (U.S.EPA, 2006) that is intentionally transferred through an AOP reactor. The reactor irradiation dose is obtained from a linear AOP dose vs. inactivation degree curve of the same surrogate previously determined in a bench-scale reactor. Chemical actinometry is an AOP-induced reaction for which the quantum yield (number of molecules changed divided by number of adsorbed photons) is accurately known. Previous reports have stated that dyes such as methylene blue and azo dyes (Neamtu et al., 2002; Alpert et al., 2010; Keen et al., 2014; Misra et al., 2015) are decolorized (bleached) by hydroxyl radical attacks on aromatic rings within the dye structure. At the same time, the dyes typically do not undergo direct photolysis and are not reactive with H_2O_2 alone. Hence, these dyes can be used as probes in light-based hydroxyl-radical systems.

Dose-responsive curves for the degradation of the fluorescence intensity of fluorescent dyes is a common way of tracing photocatalytic degradation activity under UV and visible light. Rhodamine B (RhB) is the most frequently used dye for this purpose and became known after a publication on its photo-oxidation with titanium dioxide (TiO_2) (Wu et al., 1998). RhB has been tried on many new photocatalysts ever since (Shenawi-Khalil et al., 2011; Jiang et al., 2014; Ma et al., 2014; Qi et al., 2014; Tang et al., 2014; Zhou et al., 2014).

RhB can also be used as an indicator of AOP disinfection efficiency. The degradation of RhB by hydroxyl radicals in a UV/H_2O_2 system was studied in a bench-scale quasi-collimated beam apparatus equipped with low-pressure (LP) lamps (Timchak and Gitis, 2012; Kwon et al., 2014), in an approach similar to passive spiking tests with fluorescent microspheres (Bohrerova et al., 2005; Fang et al., 2008). In Timchak and Gitis (2012), viruses were colored with RhB to emulate the behavior of actual colloidal particulate pollutants and further investigate the distribution of radicals in a disinfection reactor. Due to high diffusion coefficients, solutes spread more evenly in disinfection reactors and more accurately predicted irradiation dose at each point. “Lazy” microorganisms search for shortcuts and often leave a reactor much earlier than dictated by their hydraulic residence time, thus receiving low irradiation doses (Asraf-Snir and Gitis, 2011). However, dyed viruses are applicable not only in disinfection/oxidation studies. The advantages of colored viruses include simple quantitation by optical methods, unbiased signals even when virus aggregates are formed, and the ability to decouple inactivation kinetics from transport phenomena. Additionally, the signal reflects the removal and transport of the studied microorganism and not a surrogate (Gitis et al., 2002a). Relevant transport properties of RhB-labeled phages are practically identical to those of the native bacteriophages (Gitis et al., 2002a, b). The RhB-dyed bacteriophages were found sensitive for detection of nanometric scale breaches in the active layer of ultrafiltration membranes, and able to provide a basis for on-line testing for removal of virus-sized particles (Gitis et al., 2006). RhB-labeled phages can be used to accurately predict viral fate in porous media. When the native phages are experiencing both accumulation and inactivation, the labeled ones are inactivated already and therefore can only be accumulated. Thus the effect of inactivation is applicable to native bacteriophages only and depletion of phage concentration due to inactivation can be elucidated from a total phage balance (Gitis et al., 2011).

As detailed above, RhB-dyed bacteriophages have been used in investigations of deep-bed filtration systems, ultrafiltration membranes and chlorination reactors (Gitis et al., 2002a, b; Gitis et al., 2006; Gitis et al., 2011) and in monochromatic LP light based systems but not in polychromatic medium-pressure (MP) UV photolysis, polychromatic based UV/H_2O_2 or solar based photocatalytic systems. The developed dyeing technique (Gitis et al., 2002a) ensures that no free RhB remains in solution and therefore the fluorescence intensity can be directly linked to the amount of dyed viruses.

The complexity of AOPs and a vast variety of independent variables call for the development of a versatile monitoring system using simple indicators to track AOP performance. Especially troubling is the absence of indicators capable of tracking radicals in a flow-through reactor. The objective of our study was to demonstrate dose-response degradation of RhB by a polychromatic light-based homogeneous and heterogeneous AOP with a focus on the differences between free and nano-bound dye indicators. In addition, this study evaluated the use of bismuth oxyhalide based photocatalyst that has been recently studied due to its excellent properties and non-toxic nature of the bismuth element, however it is less commonly used (Natarajan et al., 2016; Henríquez et al., 2017) compared to TiO_2 catalyst.

2. Materials and methods

2.1. Materials and reagents

2.1.1. RhB

A 250 mg L^{-1} stock solution of RhB ($C_{28}H_{31}ClN_2O_3$; 9-(o-carboxyphenyl)-6-(diethylamino)-3H-xanthen-3-ylidene) diethylammonium chloride) was prepared by dissolving 0.0625 g of RhB powder (Aldrich) in 250 ml deionized (DI) water (Direct-Q3 UV system, Millipore-France).

The relative absorption spectrum of free (dissolved) RhB is presented in Fig. 1.

2.1.2. Degussa P25

Technical grade TiO_2 (Degussa P25; anatase/rutile particles of 21 nm average size, ~50 m^2 g^{-1} surface area measured by Brunauer–Emmett–Teller method, nonporous) was used as a reference catalyst. The feed suspension was prepared from 0.01 g of the

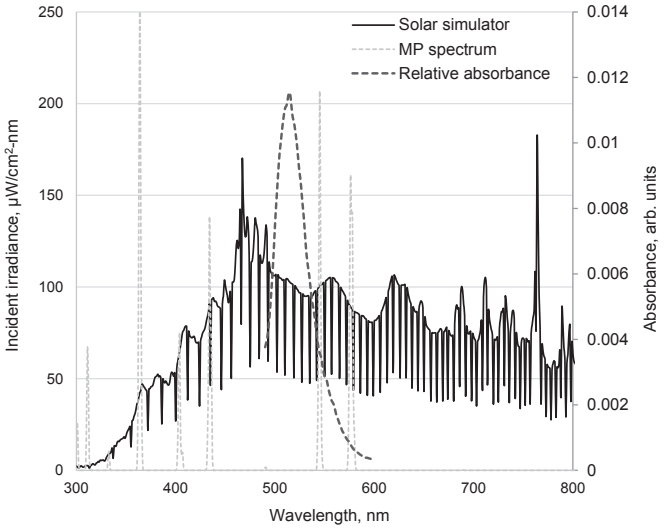

Fig. 1. Absorption spectrum of free rhodamine B and irradiation spectrum of medium-pressure (MP) UV and xenon arc lamp (solar simulator).

catalyst suspended in 10 ml of DI water and sonicated for 1 min in an ultrasonic bath. Fresh solutions were prepared before each experiment.

2.1.3. $BiOCl_{0.875}Br_{0.125}$

The bismuth-based catalyst was kindly provided by Prof. Sasson laboratory which synthesized and characterized the catalyst as described in Gnayem and Sasson (2013). Briefly, the catalyst was prepared from bismuth nitrate and surface-active quaternary ammonium salts (such as cetyltrimethylammonium halides), in the presence of acetic acid as a co-solvent. The resultant powder, composed of hierarchical flower-like microspheres, was filtered, washed with water and ethanol, and dried under ambient conditions. The ammonium salts served as both bromide and chloride sources as well as structure-directing agents. The acidic conditions allowed complete dissolution of the bismuth nitrate and an instant reaction with the halide anions at room temperature, yielding the desired bismuth oxyhalide product. The size distribution of the bismuth particles was relatively narrow (mostly between 1 and 10 μm, with $d_{0.5}$ of 3.2 μm) (Sherman et al., 2016).

The Cl^-/Br^- ratio in the catalyst of 0.875/0.125 showed the best potential for RhB degradation in comparison to other ratios investigated by Gnayem and Sasson (2013). Therefore, the optimized formula $BiOCl_{0.875}Br_{0.125}$ was used in the present study. $BiOCl_{0.875}Br_{0.125}$ (10 mg) was dissolved in 10 ml DI water to obtain a 1 g L^{-1} stock solution. The solution was sonicated for 1 min to produce a homogeneous, aggregate-free suspension. Fresh solutions were prepared before each experiment.

2.2. Preparation of fluorescence-labeled bacteriophages

A detailed description of bacteriophage cultivation, enumeration and tagging is provided in (Gitis et al., 2002a, b). Briefly, MS2 and T4 bacteriophages were labeled by mixing 0.2 g of DEC (1-[3-(dimethylamino) propyl]-3-ethylcarbodiimide hydrochloride; Aldrich) coupling agent and 0.02 g of RhB in 25 ml of bacteriophage stock solution in phosphate buffer (pH 5.6). This procedure resulted in permanent attachment of the dye to the phage surface. The labeled bacteriophage mixture was then purified by membrane dialysis (MWCO = 6000–8000 Da, Scientific Instrument Center Ltd., London, UK) under stirring to remove low-molecular-weight organic compounds and free dye molecules. Comprehensive characterization (Gitis et al., 2002a) of the obtained suspension showed that the labeled probe maintains all of the properties of the native phages, except for viability.

2.3. Analytical methods

2.3.1. UV dose measurements

The average UV irradiance was calculated using the approach described in Bolton and Linden (2003), where the incident irradiance at each wavelength measured with a calibrated spectroradiometer (USB4000 Ocean Optics, FL, USA) was weighted by the spectral absorbance (with or without H_2O_2 addition), reflection at the sample surface and the measured petri factor for the dish. The integrated average irradiance over the wavelength range 220–400 nm (E_{avg}, mW cm^{-2}) was multiplied by the exposure time t (s) to provide the UV dose (fluence) in mJ cm^{-2}.

2.3.2. Fluorescence intensity measurement

Fluorescence intensity was measured with Synergy HT (Bio Tek Instruments) fluorimeter equipped with a tungsten halogen lamp. Samples were held in a flat-bottomed black 96-well plate (Nunc™, Thermo Scientific). Samples (100 μl) were placed in the 400-μl wells under dark conditions and were held covered from any light source until measurement. At least two wells were examined for each time interval tested.

The intensity was reported in the instrument's relative fluorescence units (RFU), calculated by Synergy fluorimeter software which interprets the results from the fluorescence intensity of each data point. Excitation was at 530 nm (25-nm bandwidth) and emission at 590 nm (20-nm bandwidth).

2.4. Experimental setup

2.4.1. Direct UV photolysis and UV/H_2O_2 AOP

Direct UV photolysis and UV/H_2O_2 AOP experiments were conducted in a completely mixed collimated beam apparatus. The AOP tests were performed with the addition of H_2O_2 at concentrations between 0 and 100 mg L^{-1}. Tests were carried out using a 450-W polychromatic (200–400 nm) MP Hg vapor lamp (Ace-Hanovia No. 7830-61, Ace Glass Inc.) housed in a quasi-collimated beam apparatus at room temperature. The UV radiation was directed through a circular opening (collimated tube) to provide incident radiation normal to the surface of the tested suspension. Suspensions (10 ml) were embedded in 5.3-cm diameter, 1.2-cm deep petri dishes and gently stirred during irradiation. The total exposed surface area of 22 cm^2 and the average 0.5-cm suspension depth were calculated based on the above information. Ace Glass Inc. provided the total UV radiated energy of 83 W and UV power of 1.15 W cm^{-2} at the lamp surface was calculated.

2.4.2. Photocatalysis

A 150-W ozone-free xenon arc lamp (Sciencetech Inc., Canada) was used with a maximum optical output irradiance given by the manufacturer of 1000 W m^{-2}, after the light beam was filtered through a 1.5 global air mass filter. The output spectrum of the solar simulator was equivalent to natural sunlight at 48.2° latitude at sea level. The solar simulator setup, calibration and spectrum were as previously described (Theitler et al., 2012; Lester et al., 2014). The irradiation spectrum of the MP UV and xenon arc lamp is presented in Fig. 2. Solar irradiance was measured by a calibrated spectroradiometer (International Light, Model ILT 900R, USA). Total incident irradiance, integrated between 280 and 950 nm, was ~550 W m^{-2}.

Experiments were performed with free or nano-bound RhB and various amounts of catalyst suspended in 10 ml DI water and gently

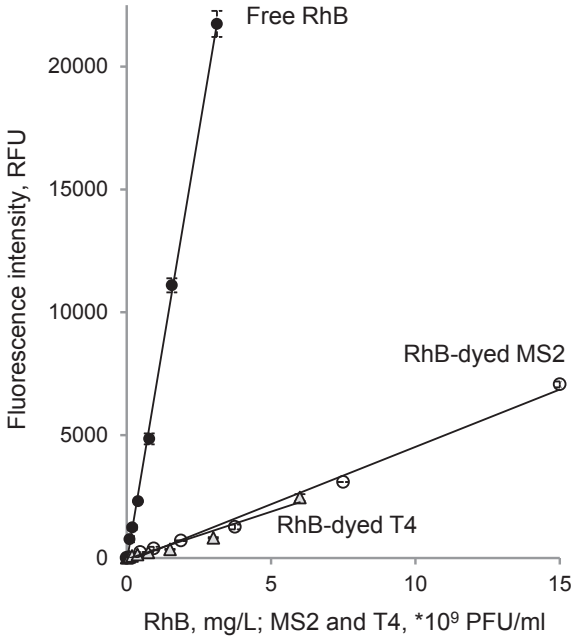

Fig. 2. Changes in fluorescence intensity as a function of concentration of 0–3.13 mg/l free rhodamine B (RhB) (full circles), 0–15 × 10^9 PFU ml^{-1} RhB-dyed MS2 (empty circles) and 0–6 × 10^9 PFU ml^{-1} RhB-dyed T4 (empty triangles).

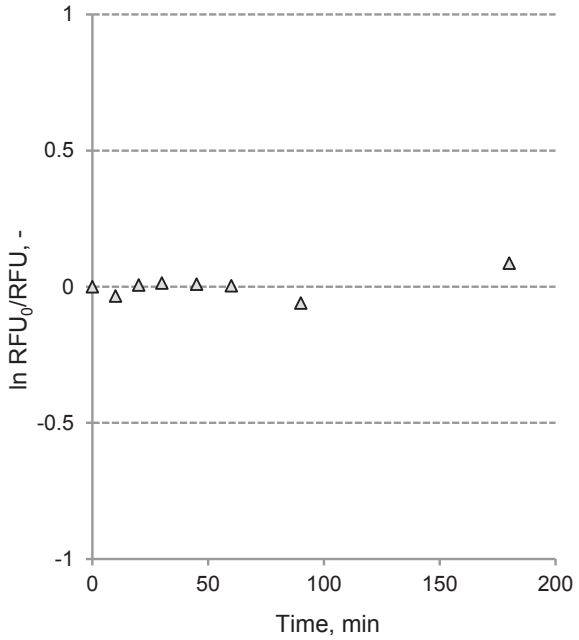

Fig. 3. Changes in fluorescence intensity of 1 mg L^{-1} free rhodamine B (pH = 5.58) exposed to 100 mg L^{-1} H_2O_2 in the dark, as a function of time (pH = 5.58, with up to 100 mg L^{-1} H_2O_2).

stirred during the tests. In experiments with free RhB, the spent catalyst was centrifuged out at 20,020 rcf (g) for 10 min after the test (Eppendorf, Model 5424, Hamburg, Germany). The centrifugation was performed to ensure no catalyst fluorescence intensity at RhB excitation/emission wavelengths.

3. Results and discussion

3.1. RhB degradation by UV/H_2O_2 AOP

Fig. 2 depicts changes in fluorescence intensity of free and nano-bound RhB as a function of their concentration. Free and nano-bound RhB displayed linear curves throughout the examined concentration range. Pearson's R-square (correlation coefficient) values were above 0.99 for all probes. High linearity of calibration curves is critical for a rapid and accurate determination of concentrations of free dyes and viruses in AOP reactors. The fluorescence intensity of free RhB changed more sharply in response to concentration changes, thus showing a higher sensitivity of free dyes. The difference in sensitivity could be attributed to partial amortization of the fluorescence signal by the outer virus capsid. Similar changes in fluorescence intensity of 0–3.13 mgL^{-1} free RhB, 0–15 × 10^9 PFU ml^{-1} nano-bound MS2 and 0–6 × 10^9 PFU ml^{-1} nano-bound T4 viruses in response to concentration changes support this claim.

Fig. 3 shows changes in fluorescence intensity of 1 mg L^{-1} free RhB mixed with 100 mg L^{-1} H_2O_2 in the dark as a function of time. There was no degradation of free dye with H_2O_2 in the dark, even after 3 h.

The decomposition of RhB occurs under UV light due to a combined effect of direct UV photolysis and indirect photo-oxidation by •OH radicals formed from H_2O_2 by UV light. Assuming a total first-order decomposition rate, the degradation of RhB can be described as

$$\ln\frac{[RhB]_0}{[RhB]_t}\Big/ t = k_{obs} = k' + k_{\bullet OH}\,[\bullet OH] \tag{1}$$

where $[RhB]_0$ and $[RhB]_t$ are initial RhB concentration (M) and its concentration after exposure time t (s), respectively, k_{obs} is the observed (total) degradation rate constant (s^{-1}), $k_{\bullet OH}$ is the radical decomposition rate constant (s^{-1} M^{-1}), [•OH] is the concentration of hydroxyl radicals (M), and k' is the direct UV light degradation rate constant (s^{-1}). The latter is calculated under the assumption of excessive UV light as

$$k' = \varphi_{RhB} \times k_{s,RhB} \tag{2}$$

$$k_{s,RhB} = \sum_{200-400} \frac{10^{-3} \times E_p^0(\lambda)\varepsilon_{RhB}(\lambda)\left[1 - 10^{-a(\lambda)z}\right]}{a(\lambda)z} \tag{3}$$

where Φ_{RhB} is the quantum yield for RhB removal (M $Einstein^{-1}$) and $k_{s,RhB}$ is the specific rate of light absorption by RhB (Einstein s^{-1} M^{-1}). E^0p (λ) is the incident photon irradiance (Einstein s^{-1} cm^{-2}), ε_{RhB} (λ) is the molar absorption coefficient of RhB (M^{-1} cm^{-1}), a (λ) is the solution absorption coefficient (cm^{-1}) and z is the solution depth (cm). RhB degradation due to UV photolysis and radical decomposition was calculated by comparing k' and $k_{\bullet OH}$. Independent evaluation of k' included the calculation of a $k_{s,RhB}$ value of 0.0278 E s^{-1} M^{-1} using Eq. (3) followed by derivation of Φ_{RhB} of 0.018 M E^{-1} from a UV slope (the calibration figure is not shown). The resulting k' was 5 × 10^{-4} s^{-1} (Eq. (2)). The concentration of •OH radicals was derived following the procedure described in (Lester et al., 2010). Relevant $k_{\bullet OH}$ values were 1.3 × 10^{10} s^{-1} M^{-1} for 10 mg L^{-1} H_2O_2 and 7.7 × 10^{-13} M •OH, 6.42 × 10^9 s^{-1} M^{-1} for 25 mg L^{-1} H_2O_2 and 1.9 × 10^{-12} M •OH, and 4.9 × 10^9 s^{-1} M^{-1} for 50 mg L^{-1} H_2O_2 and 2.4 × 10^{-12} M •OH. Fig. 4 shows the total degradation rate constant (k_{obs}) as a function of

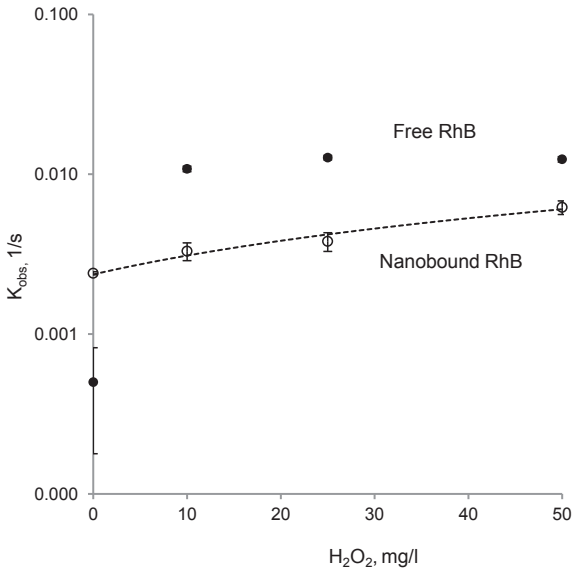

Fig. 4. Total degradation rate constant (k_{obs}) as a function of H_2O_2 concentration, for 1 mg L^{-1} free and 4 × 10^9 PFU ml^{-1} nano-bound RhB by UV irradiation and AOP.

H_2O_2 concentration, for 1 mg L^{-1} free and 4 × 10^9 PFU ml^{-1} nano-bound T4 RhB.

The direct degradation of free RhB by MP UV light only showed a minor k_{obs} (or k') of 5 × 10^{-4} s^{-1}. This is because direct photochemical reaction with an organic substance requires an absorption spectrum that overlaps with the spectrum of the incoming radiation. The k_{obs} (or k') of direct nano-bound RhB degradation by MP UV was 2.4 × 10^{-3} s^{-1}. Experiments performed with the addition of 10, 25 and 50 mg L^{-1} H_2O_2 resulted in significant degradation of both free and nano-bound forms of RhB. The total degradation rate of nano-bound RhB depended linearly on H_2O_2 dose with an R^2 of 0.97. The degradation rate of free RhB at 25 mg L^{-1} H_2O_2 was similar to that at 50 mg L^{-1}. Higher decomposition of free dyes was observed for the entire H_2O_2 range, as expected. Timchak and Gitis (2012) reported similar trends of minor RhB degradation with direct UV photolysis in a LP collimated beam apparatus (emitting at 254 nm) and accelerated reaction with the addition of H_2O_2.

A possible explanation for the differences in indicator performance might be the radicals' accessibility to the dye. Free RhB is more accessible to •OH radical oxidation, whereas in the bacteriophages the dye is conjugated, and therefore the photons emitted in direct UV photolysis and the •OH radicals created in AOP can degrade other available sites of the nano-bound indicator, resulting in weaker attenuation of RhB measured as higher fluorescence intensity of the solution.

Timchak and Gitis (2012) assumed that each dyed virus contains approximately 52 dye molecules and reported that limited availability of •OH radicals and their preferential participation in virus inactivation are possible reasons for lower bleaching of fluorescent dyes in the presence of viruses. An additional explanation is related to the different surface areas of the indicators. While free dye molecules are dissolved in solution, MS2 bacteriophages are nanometrically scaled, meaning that their volume-to-surface area ratio is smaller than for free molecules. This diversity could influence indicators' statistical chances of being degraded by direct UV photolysis and UV/H_2O_2 AOPs. Degradation of RhB-dyed viruses (nano-bound RhB) requires higher H_2O_2 concentrations and longer irradiation periods.

3.2. RhB degradation by solar irradiation in the presence of a catalyst

Following the linear degradation of RhB in UV/H_2O_2 AOP reported in section 3.1, a series of experiments was executed to examine the validity of free and nano-bound RhB as indicators for solar-based AOP. In this situation, sunlight is mimicked by a 150-W xenon arc lamp solar simulator, and RhB degradation occurs in the presence of the heterogeneous catalysts TiO_2 or $BiOCl_{0.875}Br_{0.125}$. The RhB degradation is calculated as percent reduction of free RhB fluorescence intensity:

$$RhB\ degradation = \left[\frac{RFU_0 - RFU_t}{RFU_0}\right] \times 100\% \quad (4)$$

where RFU_0 is the fluorescence intensity before irradiation and RFU_t is the intensity at time t. Twenty, 45, 56, 67 and 87% RhB degradation was received after 2, 6, 8, 10, 15 min of an experiment performed in presence of 0.5 g L^{-1} bismuth. An addition of 1 g L^{-1} bismuth resulted in 24, 51, 66, 81 and 98% RhB degradation at the same time intervals. Finally, an addition of 1.5 g L^{-1} bismuth resulted in 29, 57, 76, 90, 99% degradation. The initial RhB concentration was 25 g L^{-1}.

The degradation of free RhB depended directly on time and catalyst concentration. The dependence was linear for 0.5 and 1 g L^{-1} bismuth with R^2 values of 0.98 and 0.97, respectively, and almost linear for 1.5 g L^{-1} bismuth with R^2 of 0.91. A deviation from linearity was seen at long irradiation times. A gap in RhB degradation between various catalyst concentrations was also significant at prolonged irradiation times. An average 5% gain in RhB degradation when bismuth concentration was changed gradually from 0.5 to 1.5 g L^{-1} was obtained at 2 and 6 min. A 10% gain was observable at 8 min irradiation. At longer times, the transition from 0.5 to 1.5 g L^{-1} bismuth resulted in over 20% higher RhB degradation. A higher number of available active catalyst sites for light

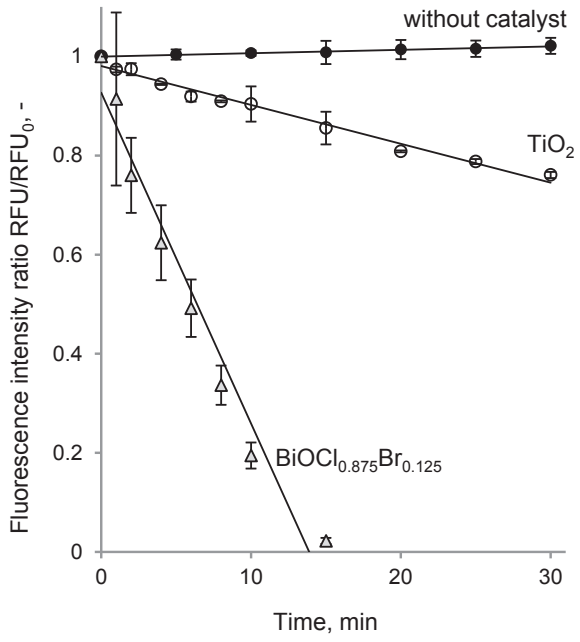

Fig. 5. Changes in fluorescence intensity of 25 mg/l free rhodamine B as a function of irradiation time using a 150-W xenon arc lamp solar simulator. Experiments were performed without catalyst (full circles) (pH 4.51), with addition of 1 g L^{-1} TiO_2 (empty circles) (pH 4.70), and with addition of 1 g L^{-1} bismuth (empty triangles) (pH 4.88). Initial fluorescence intensity of RhB was 50,000 RFU (Synergy fluorimeter).

absorption (Lester et al., 2014) is a possible reason for the higher degradation at increased catalyst concentration. Further experiments were performed with 1 g L^{-1} bismuth and 1 g L^{-1} TiO_2.

Fig. 5 illustrates the attenuation of the fluorescence intensity of 25 g L^{-1} free RhB by solar light with and without the addition of 1 g L^{-1} TiO_2 or 1 g L^{-1}bismuth catalysts, as a function of irradiation time. No RhB degradation was observed in the absence of catalyst.

In general, photocatalyzed decolorization of a dye can proceed through three mechanisms. The first is formation of an electron–hole pair on the catalyst surface by a direct photocatalytic process in which UV irradiation ($\lambda \leq 385$ nm) promotes an electron from its valence band to a conduction band:

$$(MO/MO_2) + hv \rightarrow (MO/MO_2)\,(e^-_{cb} + h^+_{vb}) \quad (5)$$

A high oxidation potential of the hole h^+_{vb} promotes direct RhB oxidation:

$$h^+_{vb} + RhB \rightarrow RhB^+ \rightarrow RhB\ oxidation \quad (6)$$

The second mechanism is excitation of a dye electron and its injection into the conduction band of a photocatalyst by photosensitization processes (Sanchez Martinez et al., 2011; Li et al., 2012) under visible light irradiation. In a previous study, Gnayem and Sasson (2013) reported that RhB degradation under visible light proceeds through light adsorption by RhB. The emitted electron is transferred to bismuth and adsorbed by an electron acceptor on the catalyst surface. In another study (Sherman et al., 2016), high oxidation potential of the hole h^+_{vb} promoted direct bacterial oxidation of *Escherichia coli* by adsorption of the bacteria onto the catalyst surface for their further degradation.

The third mechanism is the generation of hydroxyl radicals from water by electron holes:

$$h^+_{vb} + H_2O \rightarrow H^+ + {}^{\bullet}OH \quad (7)$$

$${}^{\bullet}OH + RhB \rightarrow RhB\ degradation \quad (8)$$

Addition of TiO_2 resulted in only 24% RhB degradation after 30 min. This minor degradation could be partially attributed to a jump in the fluorescence intensity from 50,000 RFU to 75,000 RFU immediately after catalyst addition. A drop from 50,000 RFU to 29,000 RFU was observed with the addition of bismuth catalyst. Both of these sharp shifts were addressed by adjusting initial RFU values. The addition of bismuth resulted in significantly better RhB decomposition, up to complete disappearance after just 15 min. Better performance of bismuth over TiO_2 under the same irradiation conditions has also been reported by Shenawi-Khalil et al. (2011).

The sudden reduction in fluorescence intensity of free RhB upon addition of bismuth catalyst was further examined. Fig. 6 depicts changes in fluorescence intensity of 25 mg L^{-1} free RhB after addition of 1 g L^{-1} bismuth and 1 g L^{-1} TiO_2 catalysts in the dark (with no solar irradiation).

The addition of TiO_2 resulted in a slight (3%) increase in free RhB fluorescence intensity after 90 min. The addition of bismuth catalysts resulted in a continuous reduction in free RhB fluorescence intensity, down to 57% of the initial intensity by the end of the experiment. The reduction was not linear and essentially ended after 30 min. Interestingly, in an additional experiment performed with 100-fold reduced conc. of 0.25 g L^{-1} free RhB and 1 g L^{-1} TiO_2, the fluorescence intensity was reduced by 45% after 90 min (data not shown). In the absence of solar-induced degradation, the observed phenomenon might be due to RhB adsorption on the catalyst surface. The adsorption is compound- and concentration-dependent, as previously suggested by Lester et al. (2014). Those researchers compared the degradation of carbamazepine (an antiepileptic drug) in the presence of TiO_2 and bismuth catalysts and reported more significant adsorption on the latter. Catalytic degradation of RhB requires adsorption of the dye on the catalyst surface. The generation of electron holes in a direct photocatalytic process and through photosensitization occurs on the catalyst surface and the decomposition of neighboring adsorbed RhB molecules is higher than the decomposition of free-floating RhBs. The decomposition of adsorbed RhB constantly reduces its concentration on the catalyst surface, stimulating the diffusion of free-floating RhB toward the catalyst surface, and its further degradation. Indirect proof of the described phenomenon was received from a subsequent experiment, detailed in Fig. 7.

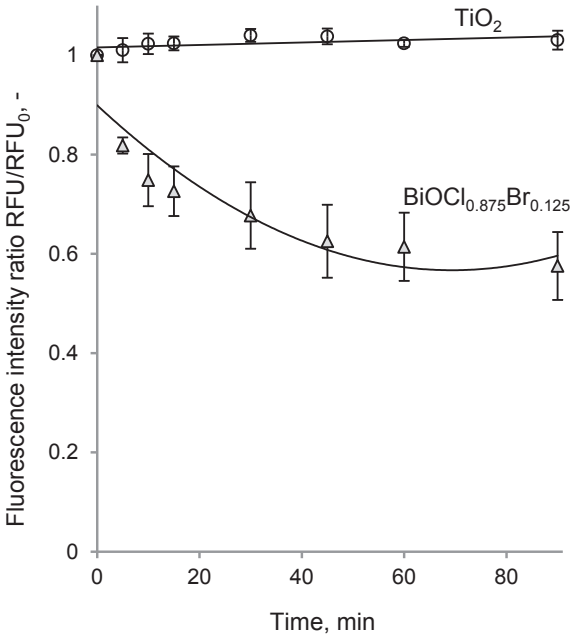

Fig. 6. Changes in fluorescence intensity of 25 mg L^{-1} free rhodamine B as a function of time due to adsorption to 1 g L^{-1} TiO_2 (circles) and 1 g L^{-1} bismuth ($BiOCl_{0.875}Br_{0.125}$; triangles) in the dark.

Fig. 7 depicts changes in fluorescence intensity of 3.75×10^9 PFU ml^{-1} nano-bound RhB in the presence of 1 g L^{-1} TiO_2 and of 1 g L^{-1} bismuth catalysts under solar irradiation, as a function of irradiation time. The main difference from the previous experiments was that the RhB was conjugated to MS2 viruses. A 5% decrease in RhB fluorescence intensity was observed in experiments performed in the absence of catalyst. The addition of either bismuth or TiO_2 catalysts resulted in a similar degradation of fluorescence intensity, reaching a 90% reduction after only 3–4 min. No traces of fluorescence were recorded after 4 min with bismuth and 6 min with TiO_2. Similar rapid degradation of carbamazepine was reported by Lester et al. (2014), with 80 and 65% decomposition of 1 ppb carbamazepine after 5 min solar irradiation in the presence of bismuth and TiO_2 catalysts, respectively.

Under the conditions described herein, it can be cautiously stated that of the two examined indicators, dyed MS2 bacteriophages most closely mimicked actual pollutant degradation, requiring only 3–5 min for complete degradation of the indicator under simulated solar irradiation in the presence of bismuth and TiO_2 catalysts.

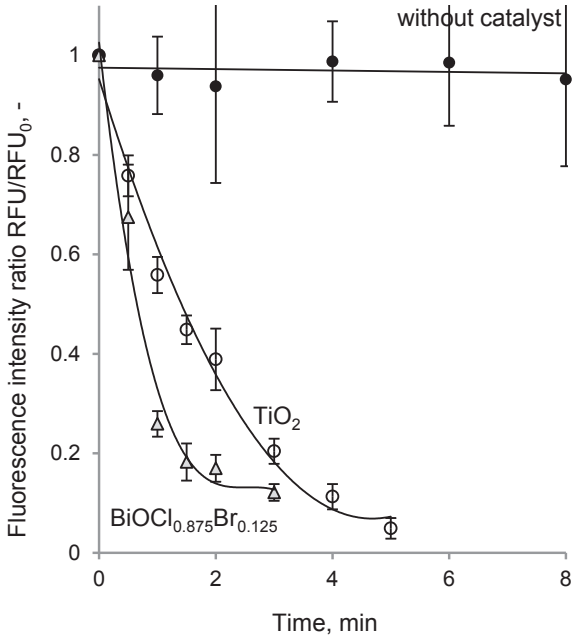

Fig. 7. Changes in fluorescence intensity of rhodamine B-dyed MS2 as a function of irradiation time using a 150-W xenon arc lamp solar simulator. Experiments were performed without catalyst (full circles), with addition of 1 g L^{-1} TiO_2 (empty circles), and with addition of 1 g L^{-1} bismuth ($BiOCl_{0.875}Br_{0.125}$; empty triangles).

4. Conclusions

Decomposition of RhB in free and nano-bound forms by •OH radicals and electron holes under UV and visible light was proven to be linear. That and the high fluorescence intensity of the initial probe, even at minor RhB concentrations, suggest an unprecedented advantage of the dye for various AOP biodosimetry needs as a valid indicator of direct UV photolysis, UV/H_2O_2 and photocatalytic processes.

Two important phenomena were observed when free and nano-bound RhB indicators were tested as indicators for photocatalytic processes:

(i) free RhB was massively adsorbed to the bismuth-based catalyst, but not the TiO_2 catalyst, at the catalyst and free dye concentrations used in this study;
(ii) adding different catalysts changed the initial fluorescence, measured before any irradiation occurred. The fluorescence of free dyes and dyed bacteriophages increased when mixed with TiO_2, and decreased when mixed with $BiOCl_{0.875}Br_{0.125}$.

High photocatalytic-degradation potential of bismuth catalyst was demonstrated not only on free (soluble) but also nano-bound RhB. The latter degraded even faster than its free-floating form. Bismuth is a benign, non-toxic element and as such, its use as a catalyst may be of extreme importance and in this research as its performance surpassed the performance of P25 TiO_2 catalysts.

Acknowledgement

Thanks to Prof. Yoel Sasson and his PhD doctoral student Hani Gnayem from the Casali Center of Applied Chemistry, The Institute of Chemistry, The Hebrew University of Jerusalem, Jerusalem, Israel, for kindly providing us with the Bismuth photocatalyst. We thank Aviv Duek for the help and guidance during initial steps of phage cultivation and dying. We also thank Dr. Yaal Lester for his advice during the study.

References

Alpert, S.M., Knappe, D.R.U., Ducoste, J.J., 2010. Modeling the UV/hydrogen peroxide advanced oxidation process using computational fluid dynamics. Water Res. 44, 1797–1808.
Asraf-Snir, M., Gitis, V., 2011. Tracer studies with fluorescent-dyed microorganisms-A new method for determination of residence time in chlorination reactors. Chem. Eng. J. 166, 579–585.
Bagheri, M., Mohseni, M., 2015. Impact of hydrodynamics on pollutant degradation and energy efficiency of VUV/UV and H2O2/UV oxidation processes. J. Environ. Manag. 164, 114–120.
Bahnmuller, S., Loi, C.H., Linge, K.L., von Gunten, U., Canonica, S., 2015. Degradation rates of benzotriazoles and benzothiazoles under UV-C irradiation and the advanced oxidation process UV/H2O2. Water Res. 74, 143–154.
Bohrerova, Z., Bohrer, G., Mohanraj, S.M., Ducoste, J., Linden, K.G., 2005. Experimental measurements of fluence distribution in a UV reactor using fluorescent microspheres. Environ. Sci. Technol. 39, 8925–8930.
Bolton, J.R., Linden, K.G., 2003. Standardization of methods for fluence (UV dose) determination in bench-scale UV experiments. J. Environ. Eng. ASCE 129, 209–215.
Ducoste, J.J., Alpert, S.M., 2015. Computational fluid dynamics modeling alternatives for UV-initiated advanced oxidation processes. Water Qual. Res. J. Can. 50, 4–20.
Fang, S., Guan, Y., Blatchley III, E.R., Shen, C., Bergstrom, D.E., 2008. Conjugation of (E)-5-2-(Methoxycarbonyl)ethenyl cytidine to hydrophilic microspheres: development of a mobile microscale UV light actinometer. Bioconjugate Chem. 19, 592–597.
Gitis, V., Adin, A., Nasser, A., Gun, J., Lev, O., 2002a. Fluorescent dye labeled bacteriophages - a new tracer for the investigation of viral transport in porous media: 1. Introduction and characterization. Water Res. 36, 4227–4234.
Gitis, V., Adin, A., Nasser, A., Gun, J., Lev, O., 2002b. Fluorescent dye labeled bacteriophages - a new tracer for the investigation of viral transport in porous media: 2. Studies of deep-bed filtration. Water Res. 36, 4235–4242.
Gitis, V., Dlugy, C., Gun, J., Lev, O., 2011. Studies of inactivation, retardation and accumulation of viruses in porous media by a combination of dye labeled and native bacteriophage probes. J. Contam. Hydrol. 124, 43–49.
Gitis, V., Haught, R.C., Clark, R.M., Gun, J., Lev, O., 2006. Nanoscale probes for the evaluation of the integrity of ultrafiltration membranes. J. Membr. Sci. 276, 199–207.
Gnayem, H., Sasson, Y., 2013. Hierarchical nanostructured 3D flowerlike $BiOCl_xBr_{1-x}$ semiconductors with exceptional visible light photocatalytic activity. ACS Catal. 3, 186–191.
Henríquez, A., Mansilla, H.D., Martínez de laCruz, A., Freer, J., Contreras, D., 2017. Selective oxofunctionalization of cyclohexane over titanium dioxide–based and bismuth oxyhalide (BiOX, X= Cl–, Br–, I–) photocatalysts by visible light irradiation. Appl. Catal. B: Environ. 206, 252–262.
Jiang, D., Zhu, J., Chen, M., Xie, J., 2014. Highly efficient heterojunction photocatalyst based on nanoporous g-C_3N_4 sheets modified by Ag_3PO_4 nanoparticles: synthesis and enhanced photocatalytic activity. J. Colloid Interface Sci. 417, 115–120.
Keen, O.S., McKay, G., Mezyk, S.P., Linden, K.G., Rosario-Ortiz, F.L., 2014. Identifying the factors that influence the reactivity of effluent organic matter with hydroxyl radicals. Water Res. 50, 408–419.
Kwon, M., Kim, S., Yoon, Y., Jung, Y., Hwang, T.-M., Kang, J.-W., 2014. Prediction of the removal efficiency of pharmaceuticals by a rapid spectrophotometric method using Rhodamine B in the UV/H_2O_2 process. Chem. Eng. J. 236, 438–447.
Lester, Y., Avisar, D., Gnayem, H., Sasson, Y., Shavit, M., Mamane, H., 2014. Demonstrating a new BiOCl0.875Br0.125 photocatalyst to degrade pharmaceuticals under solar irradiation. Water Air Soil Pollut. 225.
Lester, Y., Avisar, D., Mamane, H., 2010. Photodegradation of the antibiotic sulphamethoxazole in water with UV/H_2O_2 advanced oxidation process. Environ. Technol. 31, 175–183.
Li, J., Qiao, H., Du, Y., Chen, C., Li, X., Cui, J., Kumar, D., Wei, Q., 2012. Electrospinning synthesis and photocatalytic activity of mesoporous TiO_2 nanofibers. Sci. World. J.
Ma, P., Chen, A., Wu, Y., Fu, Z., Kong, W., Che, L., Ma, R., 2014. Ag(I)-bovine serum albumin hydrosol-mediated formation of Ag_3PO_4/reduced graphene oxide composites for visible-light degradation of Rhodamine B solution. J. Colloid Interface Sci. 417, 293–300.
Misra, N.N., Keener, K.M., Bourke, P., Cullen, P.J., 2015. Generation of in-package cold plasma and efficacy assessment using methylene blue. Plasma Chem. Plasma Process. 35, 1043–1056.
Natarajan, K., Bajaj, H.C., Tayade, R.J., 2016. Photocatalytic efficiency of bismuth oxyhalide (Br, Cl and I) nanoplates for RhB dye degradation under LED irradiation. J. Ind. Eng. Chem. 34, 146–156.
Neamtu, M., Siminiceanu, H., Yediler, A., Kettrup, A., 2002. Kinetics of decolorization and mineralization of reactive azo dyes in aqueous solution by the UV/H_2O_2 oxidation. Dyes Pigments 53, 93–99.
Oller, I., Malato, S., Sanchez-Perez, J.A., 2011. Combination of advanced oxidation

processes and biological treatments for wastewater decontamination-A review. Sci. Total Environ. 409, 4141–4166.
Qi, L., Yu, J., Liu, G., Wong, P.K., 2014. Synthesis and photocatalytic activity of plasmonic Ag@AgCl composite immobilized on titanate nanowire films. Catal. Today 224, 193–199.
Sanchez Martinez, D., Martinez-de la Cruz, A., Lopez Cuellar, E., 2011. Photocatalytic properties of WO_3 nanoparticles obtained by precipitation in presence of urea as complexing agent. Appl. Catal. Gen. 398, 179–186.
Shenawi-Khalil, S., Uvarov, V., Kritsman, Y., Menes, E., Popov, I., Sasson, Y., 2011. A new family of $BiO(Cl_xBr_{1-x})$ visible light sensitive photocatalysts. Catal. Commun. 12, 1136–1141.
Sherman, I., Gerchman, Y., Sasson, Y., Gnayem, H., Mamane, H., 2016. Disinfection and mechanistic insights of E. coli in water by bismuth oxyhalide photocatalysis. Photochem. Photobiol. 92, 826–834.
Tang, H., Zhang, D., Tang, G., Ji, X., Li, C., Yan, X., Wu, Q., 2014. Low temperature synthesis and photocatalytic properties of mesoporous TiO_2 nanospheres. J. Alloy. Compd. 591, 52–57.
Theitler, D.J., Nasser, A., Gerchman, Y., Kribus, A., Mamane, H., 2012. Synergistic effect of heat and solar UV on DNA damage and water disinfection of E. coli and bacteriophage MS2. J. Water Health 10, 605–618.
Timchak, E., Gitis, V., 2012. A combined degradation of dyes and inactivation of viruses by UV and UV/H_2O_2. Chem. Eng. J. 192, 164–170.
U.S.EPA, 2006. Ultraviolet Disinfection Guidance Manual for the Final Long Term 2 Enhanced Surface Water Treatment Rule. United States Environmental Protection, Office of Water.
Wu, T.X., Liu, G.M., Zhao, J.C., Hidaka, H., Serpone, N., 1998. Photoassisted degradation of dye pollutants. V. Self-photosensitized oxidative transformation of Rhodamine B under visible light irradiation in aqueous TiO_2 dispersions. J. Phys. Chem. B 102, 5845–5851.
Zhou, C., Shang, L., Yu, H., Bian, T., Wu, L.-Z., Tung, C.-H., Zhang, T., 2014. Mesoporous plasmonic Au-loaded Ta_2O_5 nanocomposites for efficient visible light photocatalysis. Catal. Today 225, 158–163.
Zucker, I., Avisar, D., Mamane, H., Jekel, M., Hübner, U., 2016. Determination of oxidant exposure during ozonation of secondary effluent to predict contaminant removal. Water Res. 100, 508–516.